Available online at www.sciencedirect.com
SCIENCE DIRECT®
Comput. Methods Appl. Mech. Engrg. 195 (2006) 571–587
Computer methods in applied mechanics and engineering
www.elsevier.com/locate/cma

In search of a consistent and conservative mass flux for the GWCE

T.C. Massey *, C.A. Blain

Naval Research Laboratory, Oceanography Division Code 7322, Stennis Space Center, MS 39529, USA

Received 25 August 2004; accepted 25 February 2005

Abstract

Two methods for computing local mass flux for a continuous Galerkin finite element formulation of the Generalized Wave Continuity Equation (GWCE) are derived and a third method is discussed in light of the first two. The GWCE is shown to not conserve mass locally, while it can be shown to conserve a certain quantity locally. The two derived methods are demonstrated for a realistic tidal flow problem in the Bight of Abaco, Bahamas.
Published by Elsevier B.V.

Keywords: Galerkin finite element; GWCE; Local conservation; Local mass flux

1. Introduction

The need to preserve conservation within the discrete representation of a governing conservation law is not in dispute. There are however, several ways by which the conservative properties of a particular algorithm can be evaluated. For more than a decade, the locally conservative properties of continuous Galerkin (CG) finite element formulations of the shallow water equations have been in question, see [16,12,2]. In particular mass imbalances were first observed independently in 1992 by Kolar and Westerink [9] in transient solutions obtained using the Generalized Wave Continuity Equation (GWCE) form of the primitive mass conservation law. These collective experiences have led to the conclusion that CG-based finite element solutions are not locally conservative. The mass error used to evaluate local conservation in these applications to date has typically been computed element-wise using a volumetric approach by which the discrete form of the primitive conservation law is formulated using physical arguments, see [8] for example. While

* Corresponding author. Tel.: +1 228 688 5449; fax: +1 228 688 4759.
E-mail addresses: massey@nrlssc.navy.mil (T.C. Massey), blain@nrlssc.navy.mil (C.A. Blain).

0045-7825/$ - see front matter Published by Elsevier B.V.
doi:10.1016/j.cma.2005.02.013

conceptually satisfying, this approach is inconsistent with the finite element basis and equations used to solve the GWCE itself as brought to light by Berger and Howington [3] and Hughes et al. [6]. In their work, Berger and Howington [3] show how to define partial fluxes in such a way as to be consistent with the local CG conservation statement. They also argue that with this definition of the partial flux, the CG method can be seen as locally conservative when applied to conservation laws. In recent work by Hughes et al. [6], they derive an appropriate post-processing technique that through expansion of the basis of the solution, results in a CG finite element solution that is locally conservative, i.e. on each element the conservation statement being approximated is satisfied exactly by the discrete solution. Hughes et al. [6] demonstrate that the CG method is not only globally conservative but is also locally conservative when using a strictly consistent means for evaluating conservation. To be clear, when checking mass balance, we say that a method is consistent, if it enforces mass balance in the same manner that is prescribed by the discrete equations which are solved, this includes using the same set of equations and the same basis functions as the solution itself uses.

One important distinction regarding the analyses of both Hughes et al. [6] and Berger and Howington [3] is that they are relevant to the primitive form of the continuity equation. Of particular interest here is local conservation with respect to a GWCE-based shallow water equation model. So, in light of the work of Hughes et al. [6] and Berger and Howington [3], we endeavor to examine the local conservation properties of the GWCE by constructing fluxes that are consistent with the CG statement for the GWCE, which is not an explicit conservation law. In doing so we show that the GWCE is not locally mass conservative, although it is locally conservative with respect to certain quantities.

The remainder of the paper is organized as follows: In Section 2 we briefly go through the derivation of the GWCE and cast it into an element level statement of the problem. In Section 3 we derive and discuss three ways of computing local mass fluxes. In Section 4 we give a numerical example of our local mass fluxes and the resulting local mass balance calculations. We conclude the paper with a summary of our findings and acknowledgments.

2. Derivation of the GWCE for ADCIRC

We wish to derive a consistent method of computing mass flux for the two-dimensional coastal circulation model known as ADCIRC, see [11,13]. ADCIRC solves the generalized wave continuity equation instead of the primitive form of the vertically-integrated continuity equation which is given as

$$\frac{\partial H}{\partial t}+\frac{\partial}{\partial x}(UH)+\frac{\partial}{\partial y}(VH)=0, \tag{1}$$

where $U, V=\frac{1}{H}\int_{-h}^{\zeta} u, v\,\mathrm{d}z$ is the depth-averaged velocities in the x, y directions; u, v is the vertically-varying velocities in the x, y directions; $H=\zeta+h$ is the total water column thickness; h is the bathymetric depth; ζ is the free surface departure from the geoid.

ADCIRC [11] and other CG finite element coastal circulation models, such as Lynch et al. [14], use the GWCE instead of Eq. (1) as a means of controlling spurious $2\Delta x$ oscillations that can result from identical basis functions being used for both elevation and velocity approximations, see [14,10]. One of the tradeoffs is that local mass conservation is no longer explicitly enforced by the Galerkin finite element statement. This does not present a problem in all situations of interest to the modeler, but when one wants to couple the results from the circulation model to a transport model, local mass conservation is a must. Also, for 3D computations, incorrect vertical velocity profiles can be attributed to the lack of local mass conservation in the horizontal current fields, see Luettich et al. [12].

What follows is a summary of the theoretical formulation of the GWCE, originally developed by Kinnmark [7], as formulated and solved in the 2D/3D version of ADCIRC. The details of the derivation follow closely those presented by Luettich and Westerink [13].

To start we assume that we have a horizontal computational domain $\Omega \subset \mathbb{R}^2$ and its boundary(ies) Γ, from which we create a two-dimensional unstructured finite element mesh consisting of N nodes and M non-overlapping triangular elements Δ_n such that no element crosses the physical boundary(ies) Γ and $\bigcup_{n=1}^{M} \Delta_n = \bar{\Omega}$. Additionally at each node we are given a bathymetric depth h that varies linearly between adjacent nodes. In order to derive the GWCE we begin by first differentiating Eq. (1) with respect to time and assuming a time invariant bathymetric depth $\left(\text{i.e. } \frac{\partial H}{\partial t} = \frac{\partial \zeta}{\partial t}\right)$, which leads to

$$\frac{\partial^2 \zeta}{\partial t^2} + \frac{\partial^2}{\partial t \partial x}(UH) + \frac{\partial^2}{\partial t \partial y}(VH) = 0. \tag{2}$$

Next we multiply Eq. (1) by the parameter τ_0 which may be variable in space, and add the result to Eq. (2) to get

$$\frac{\partial^2 \zeta}{\partial t^2} + \tau_0 \frac{\partial \zeta}{\partial t} + \frac{\partial^2}{\partial t \partial x}(UH) + \tau_0 \frac{\partial}{\partial x}(UH) + \frac{\partial^2}{\partial t \partial y}(VH) + \tau_0 \frac{\partial}{\partial y}(VH) = 0. \tag{3}$$

We use the chain rule and rearrange terms to get

$$\frac{\partial^2 \zeta}{\partial t^2} + \tau_0 \frac{\partial \zeta}{\partial t} + \frac{\partial \tilde{J}_x}{\partial x} + \frac{\partial \tilde{J}_y}{\partial y} - UH \frac{\partial \tau_0}{\partial x} - VH \frac{\partial \tau_0}{\partial y} = 0, \tag{4}$$

where

$$\tilde{J}_x = \frac{\partial}{\partial t}(UH) + \tau_0 UH \tag{5a}$$

$$= \frac{\partial Q_x}{\partial t} + \tau_0 Q_x \tag{5b}$$

$$= H \frac{\partial U}{\partial t} + U \frac{\partial \zeta}{\partial t} + \tau_0 UH, \tag{5c}$$

$$\tilde{J}_y = \frac{\partial}{\partial t}(VH) + \tau_0 VH \tag{6a}$$

$$= \frac{\partial Q_y}{\partial t} + \tau_0 Q_y \tag{6b}$$

$$= H \frac{\partial V}{\partial t} + V \frac{\partial \zeta}{\partial t} + \tau_0 VH, \tag{6c}$$

and $Q_x, Q_y = UH, VH$ is the x, y-directed flux per unit width.

A weighted residual method is applied to Eq. (4) by multiplying each term by a weighting function ϕ_j, to be defined later, and integrating over the horizontal computational domain Ω

$$\left\langle \frac{\partial^2 \zeta}{\partial t^2}, \phi_j \right\rangle_\Omega + \left\langle \tau_0 \frac{\partial \zeta}{\partial t}, \phi_j \right\rangle_\Omega + \left\langle \frac{\partial \tilde{J}_x}{\partial x}, \phi_j \right\rangle_\Omega + \left\langle \frac{\partial \tilde{J}_y}{\partial y}, \phi_j \right\rangle_\Omega - \left\langle UH \frac{\partial \tau_0}{\partial x}, \phi_j \right\rangle_\Omega - \left\langle VH \frac{\partial \tau_0}{\partial y}, \phi_j \right\rangle_\Omega = 0. \tag{7}$$

We then integrate by parts the terms involving $\tilde{J}_x$ and $\tilde{J}_y$ and use Eqs. (5b) and (6b) to get a weak form of Eq. (7),

$$\left\langle \frac{\partial^2 \zeta}{\partial t^2}, \phi_j \right\rangle_\Omega + \left\langle \tau_0 \frac{\partial \zeta}{\partial t}, \phi_j \right\rangle_\Omega - \left\langle \tilde{J}_x, \frac{\partial \phi_j}{\partial x} \right\rangle_\Omega - \left\langle \tilde{J}_y, \frac{\partial \phi_j}{\partial y} \right\rangle_\Omega - \left\langle UH \frac{\partial \tau_0}{\partial x}, \phi_j \right\rangle_\Omega - \left\langle VH \frac{\partial \tau_0}{\partial y}, \phi_j \right\rangle_\Omega + \int_\Gamma \left(\frac{\partial Q_N}{\partial t} + \tau_0 Q_N \right) \phi_j \partial \Gamma = 0, \tag{8}$$

where $Q_N = [Q_x, Q_y] \cdot N$ is the outward flux per unit width normal to the boundary Γ.

ADCIRC in its present formulation makes use of the non-conservative form of the vertically-integrated momentum equations given as

$$\frac{\partial U}{\partial t}+U\frac{\partial U}{\partial x}+V\frac{\partial U}{\partial y}-fV=-g\frac{\partial\left[\zeta+\frac{P_s}{g\rho_0}-\alpha\eta\right]}{\partial x}+\frac{\tau_{sx}}{H\rho_0}-\frac{\tau_{bx}}{H\rho_0}+\frac{M_x}{H}-\frac{D_x}{H}-\frac{B_x}{H}, \tag{9a}$$

$$\frac{\partial V}{\partial t}+U\frac{\partial V}{\partial x}+V\frac{\partial V}{\partial y}-fV=-g\frac{\partial\left[\zeta+\frac{P_s}{g\rho_0}-\alpha\eta\right]}{\partial y}+\frac{\tau_{sy}}{H\rho_0}-\frac{\tau_{by}}{H\rho_0}+\frac{M_y}{H}-\frac{D_y}{H}-\frac{B_y}{H}, \tag{9b}$$

where f is a Coriolis parameter, g is the acceleration due to gravity, ρ_0 is the reference density of water, α is the effective Earth elasticity factor, η is the Newtonian equilibrium tidal potential, P_s is the atmospheric pressure at the sea surface, τ_{sx}, τ_{sy} are imposed surface stresses, τ_{bx}, τ_{by} are bottom stress components, M_x, M_y are vertically-integrated lateral-stress gradients, D_x, D_y are momentum dispersion, B_x, B_y are vertically-integrated baroclinic-pressure gradients.

Now, if we substitute Eqs. (9) into Eqs. (5c) and (6c) and isolate the linear free surface gravity wave terms for computational reasons, see for example Haidvogel [4], we get

$$\tilde{J}_x=J_x-gh\frac{\partial\zeta}{\partial x}, \tag{10a}$$

$$\tilde{J}_y=J_y-gh\frac{\partial\zeta}{\partial y}, \tag{10b}$$

where

$$J_x=-Q_x\frac{\partial U}{\partial x}+-Q_y\frac{\partial U}{\partial y}+fQ_y-\frac{g}{2}\frac{\partial\zeta^2}{\partial x}-gH\frac{\partial\left[\frac{P_s}{g\rho_0}-\alpha\eta\right]}{\partial x}+\frac{\tau_{sx}}{\rho_0}-\frac{\tau_{bx}}{\rho_0}+M_x-D_x-B_x+U\frac{\partial\zeta}{\partial t}+\tau_0Q_x, \tag{11a}$$

$$J_y=-Q_x\frac{\partial V}{\partial x}+-Q_y\frac{\partial V}{\partial y}+fQ_x-\frac{g}{2}\frac{\partial\zeta^2}{\partial y}-gH\frac{\partial\left[\frac{P_s}{g\rho_0}-\alpha\eta\right]}{\partial y}+\frac{\tau_{sy}}{\rho_0}-\frac{\tau_{by}}{\rho_0}+M_y-D_y-B_y+V\frac{\partial\zeta}{\partial t}+\tau_0Q_y. \tag{11b}$$

Substituting Eqs. (10) into Eq. (8) and rearranging terms, we arrive at the weighted residual weak form of the GWCE that is solved by ADCIRC,

$$\left\langle\frac{\partial^2\zeta}{\partial t^2},\phi_j\right\rangle_\Omega+\left\langle\tau_0\frac{\partial\zeta}{\partial t},\phi_j\right\rangle_\Omega+\left\langle gh\frac{\partial\zeta}{\partial x},\frac{\partial\phi_j}{\partial x}\right\rangle_\Omega+\left\langle gh\frac{\partial\zeta}{\partial y},\frac{\partial\phi_j}{\partial y}\right\rangle_\Omega-\left\langle J_x,\frac{\partial\phi_j}{\partial x}\right\rangle_\Omega-\left\langle J_y,\frac{\partial\phi_j}{\partial y}\right\rangle_\Omega-\left\langle Q_x\frac{\partial\tau_0}{\partial x},\phi_j\right\rangle_\Omega-\left\langle Q_y\frac{\partial\tau_0}{\partial y},\phi_j\right\rangle_\Omega+\int_\Gamma\left(\frac{\partial Q_N}{\partial t}+\tau_0Q_N\right)\phi_j\partial\Gamma=0. \tag{12}$$

We recast Eq. (12) from a global statement to a local, element-wise, statement, by considering node j along with all nodes adjacent to it and the horizontal weighting function ϕ_j. The weighting function ϕ_j is defined to be equal to one at node j and equal to zero at all other nodes such that ϕ_j varies linearly between node j and the nodes adjacent to it, see Fig. 1. For future reference we define a finite element basis space $\mathscr{S}^N$ to be,

$$\mathscr{S}^N=\text{span}\{\phi_j,j=1:N\}\subset\mathscr{H}^1(\Omega), \tag{13}$$

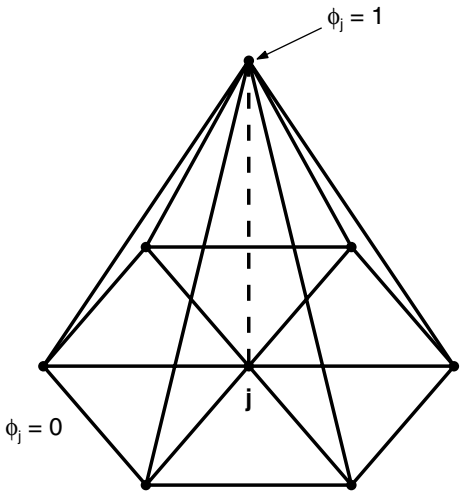

Fig. 1. Node j with adjacent nodes and the associated weight function ϕ_j.

where $\mathscr{H}^1(\Omega)$ is the usual Sobolev space consisting of all functions such that the function and its first derivatives are both square integrable over the domain Ω.

Two other important properties of the weighting function are that for any element with local node numbers $i = 1, 2, 3$ we have that the weight functions over that element sum to unity and the sum of the spatial derivatives of the weight function over the element is zero,

$$\sum_{i=1}^{3} \phi_i = 1, \tag{14a}$$

$$\sum_{i=1}^{3} \frac{\partial \phi_i}{\partial x} = 0 = \sum_{i=1}^{3} \frac{\partial \phi_i}{\partial y}. \tag{14b}$$

At this time we define some additional notations associated with node j, A_n is the area of element n, NE_j is the number of elements containing node j, Δ_n^j is the local element number n which contains node j, $\Omega_j = \bigcup_{n=1}^{NE_j} \Delta_n^j$ is the union of all the elements containing node j, Γ_j is the boundary of Ω_j, Γ_n^j is the total boundary of local element number n, $\tilde{\Gamma}_n^j$ is a two edge inner-element partial boundary of element Δ_n^j.

Using this new notation and the definition of ϕ_j we see that the integrations performed in Eq. (12) over the entire domain Ω can be reduced to integrations over the patch Ω_j, which corresponds precisely with the region over which $\phi_j \neq 0$,

$$\begin{aligned} &\left\langle \frac{\partial^2 \zeta}{\partial t^2}, \phi_j \right\rangle_{\Omega_j} + \left\langle \tau_0 \frac{\partial \zeta}{\partial t}, \phi_j \right\rangle_{\Omega_j} + \left\langle gh \frac{\partial \zeta}{\partial x}, \frac{\partial \phi_j}{\partial x} \right\rangle_{\Omega_j} + \left\langle gh \frac{\partial \zeta}{\partial y}, \frac{\partial \phi_j}{\partial y} \right\rangle_{\Omega_j} - \left\langle J_x, \frac{\partial \phi_j}{\partial x} \right\rangle_{\Omega_j} - \left\langle J_y, \frac{\partial \phi_j}{\partial y} \right\rangle_{\Omega_j} \\ &\quad - \left\langle Q_x \frac{\partial \tau_0}{\partial x}, \phi_j \right\rangle_{\Omega_j} - \left\langle Q_y \frac{\partial \tau_0}{\partial y}, \phi_j \right\rangle_{\Omega_j} + \int_{\Gamma_j} \left(\frac{\partial Q_N}{\partial t} + \tau_0 Q_N \right) \phi_j \partial \Gamma_j = 0. \end{aligned} \tag{15}$$

We note that $\int_{\Gamma_j} \left(\frac{\partial Q_N}{\partial t} + \tau_0 Q_N\right) \phi_j \partial \Gamma_j = 0$ whenever node j does not lie on the physical boundary Γ, thus Eq. (15) is equivalent to Eq. (12). Also due to cancellation

$$\int_{\Gamma_j}\left(\frac{\partial Q_N}{\partial t}+\tau_0 Q_N\right)\phi_j\partial\Gamma_j=\sum_{n=1}^{NE_j}\int_{\Gamma_n^j}\left(\frac{\partial Q_N}{\partial t}+\tau_0 Q_N\right)\phi_j\partial\Gamma_n^j. \tag{16}$$

So we rewrite Eq. (15) using elemental notation as

$$\sum_{n=1}^{NE_j}\left\{\begin{array}{l}\left\langle\frac{\partial^2\zeta}{\partial t^2},\phi_j\right\rangle_{\Delta_n^j}+\left\langle\tau_0\frac{\partial\zeta}{\partial t},\phi_j\right\rangle_{\Delta_n^j}+\left\langle gh\frac{\partial\zeta}{\partial x},\frac{\partial\phi_j}{\partial x}\right\rangle_{\Delta_n^j}+\left\langle gh\frac{\partial\zeta}{\partial y},\frac{\partial\phi_j}{\partial y}\right\rangle_{\Delta_n^j}\\ \quad-\left\langle J_x,\frac{\partial\phi_j}{\partial x}\right\rangle_{\Delta_n^j}-\left\langle J_y,\frac{\partial\phi_j}{\partial y}\right\rangle_{\Delta_n^j}-\left\langle Q_x\frac{\partial\tau_0}{\partial x},\phi_j\right\rangle_{\Delta_n^j}\\ \quad-\left\langle Q_y\frac{\partial\tau_0}{\partial y},\phi_j\right\rangle_{\Delta_n^j}+\int_{\Gamma_n^j}\left(\frac{\partial Q_N}{\partial t}+\tau_0 Q_N\right)\phi_j\partial\Gamma_n^j\end{array}\right\}=0, \tag{17}$$

which is the element level spatial discretization of the GWCE with respect to the weight function ϕ_j.

3. In search of a consistent and conservative flux

In this section we formulate two ways of computing local mass fluxes and the resulting computation of mass error. We then discuss a third approach in light of the other two.

3.1. Finite volume flux

We begin with a simple and straightforward way of computing local mass fluxes and the resulting computation of mass error. This method is commonly used, see for example [8,5,2], easy to compute and gives a physically realistic mass flux, in that it is defined normal to an element's edge. The local mass flux defined in this section is akin to one used by Kolar et al. [8] except we do not integrate in time.

We introduce a new space $\hat{\mathscr{S}}^M\subset\mathscr{L}^2(\Omega)$, such that $\hat{\mathscr{S}}^M=\text{span}\{w_n : n=1:M\}$ where $w_n(x,y)$ is equal to one wherever $(x,y)\in\Delta_n$ and zero everywhere else. We begin with a weak statement of the primitive form of the continuity equation (1) over an arbitrary element Δ_n,

$$\left\langle\frac{\partial\zeta}{\partial t},w_n\right\rangle_{\Delta_n}+\left\langle\frac{\partial}{\partial x}(UH),w_n\right\rangle_{\Delta_n}+\left\langle\frac{\partial}{\partial y}(VH),w_n\right\rangle_{\Delta_n}=0, \tag{18}$$

where $w_n(x,y)|_{\Delta_n}=1$. Next we integrate the second and third terms by parts and rearrange to get,

$$\int_{\Gamma_n}Q_N w_n\partial\Gamma_n=-\left\langle\frac{\partial\zeta}{\partial t},w_n\right\rangle_{\Delta_n}. \tag{19}$$

Thus, we define the first of our local mass fluxes, what we will call a finite volume flux, as

$$P_{\text{fv}}^n=\int_{\Gamma_n}Q_N w_n\partial\Gamma_n. \tag{20}$$

We can evaluate this mass flux directly over any edge of any element using the computed finite element solution. This mass flux is uniquely defined by the nodal values at the endpoints of an element edge, which means that the edge flux from neighboring elements will differ only in sign, due to the outward normals. However, this method is not consistent with the finite element statement solved in ADCIRC in that it is derived from Eq. (1) rather than Eq. (17) which is solved by ADCIRC, furthermore, the weight function, $w_n\in\hat{\mathscr{S}}^M$ is not part of the original basis space, $\mathscr{S}^N$. As a result local mass balance in the context of this flux is not guaranteed, by this we mean that if we evaluate Eq. (19) directly from the GWCE-based computed solution, we will not in general obtain equality.

This method remains attractive because the resulting fluxes are physically realistic, it is easy to compute, and as Kolar et al. [8] note, it is a good indicator of a methods ability to conserve mass.

3.2. A consistent flux

Since the finite volume flux is inconsistent with our finite element statement, we also consider a local mass flux that is defined in a manner consistent with the finite element formulation of the GWCE. This approach is similar to one proposed by Berger and Howington [3] for conservation laws in primitive form.

We seek to derive a consistent elemental flux from the discrete, local form of the GWCE given in Eq. (17). In a fashion similar to that detailed by Berger et al. [3], we consider a node j and its adjacent neighbors which form the patch Ω_j. We present in Fig. 2 an exploded view of the patch Ω_j, where we have extracted element Δ_1^j in order to show the edge fluxes along the inner element boundaries, $\tilde{\Gamma}_1^j$. Note that for convenience we are using local element numbering.

We separate out the terms involving element Δ_1^j in Eq. (17) and get

$$\left\{\begin{array}{l}\left\langle\frac{\partial^2\zeta}{\partial t^2},\phi_j\right\rangle_{\Delta_1^j}+\left\langle\tau_0\frac{\partial\zeta}{\partial t},\phi_j\right\rangle_{\Delta_1^j}+\left\langle gh\frac{\partial\zeta}{\partial x},\frac{\partial\phi_j}{\partial x}\right\rangle_{\Delta_1^j}+\left\langle gh\frac{\partial\zeta}{\partial y},\frac{\partial\phi_j}{\partial y}\right\rangle_{\Delta_1^j}\\ \quad-\left\langle J_x,\frac{\partial\phi_j}{\partial x}\right\rangle_{\Delta_1^j}-\left\langle J_y,\frac{\partial\phi_j}{\partial y}\right\rangle_{\Delta_1^j}-\left\langle Q_x\frac{\partial\tau_0}{\partial x},\phi_j\right\rangle_{\Delta_1^j}\\ \quad-\left\langle Q_y\frac{\partial\tau_0}{\partial y},\phi_j\right\rangle_{\Delta_1^j}+\int_{\Gamma_1^j}\left(\frac{\partial Q_N}{\partial t}+\tau_0 Q_N\right)\phi_j\partial\Gamma_1^j\end{array}\right\}$$

$$+\sum_{n=2}^{NE_j}\left\{\begin{array}{l}\left\langle\frac{\partial^2\zeta}{\partial t^2},\phi_j\right\rangle_{\Delta_n^j}+\left\langle\tau_0\frac{\partial\zeta}{\partial t},\phi_j\right\rangle_{\Delta_n^j}+\left\langle gh\frac{\partial\zeta}{\partial x},\frac{\partial\phi_j}{\partial x}\right\rangle_{\Delta_n^j}+\left\langle gh\frac{\partial\zeta}{\partial y},\frac{\partial\phi_j}{\partial y}\right\rangle_{\Delta_n^j}\\ \quad-\left\langle J_x,\frac{\partial\phi_j}{\partial x}\right\rangle_{\Delta_n^j}-\left\langle J_y,\frac{\partial\phi_j}{\partial y}\right\rangle_{\Delta_n^j}-\left\langle Q_x\frac{\partial\tau_0}{\partial x},\phi_j\right\rangle_{\Delta_n^j}\\ \quad-\left\langle Q_y\frac{\partial\tau_0}{\partial y},\phi_j\right\rangle_{\Delta_n^j}+\int_{\Gamma_n^j}\left(\frac{\partial Q_N}{\partial t}+\tau_0 Q_N\right)\phi_j\partial\Gamma_n^j\end{array}\right\}=0. \tag{21}$$

Notice that since $\phi_j = 0$ on Γ_j, evaluating the boundary integral in Eq. (21) over Γ_1^j is equivalent to evaluating it over just $\tilde{\Gamma}_1^j$.

By examining the first bracketed expression in Eq. (21), we can ascertain the inherent definition of a flux like quantity from the finite element statement, similar to what Berger and Howington [3] observed in their

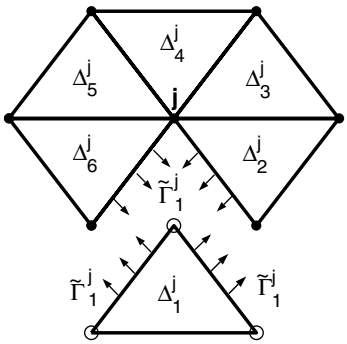

Fig. 2. The patch Ω^j with, Δ_1^j separated to show edge fluxes.

work. Thus, we define a partial numerical "flux" $P^1_{c_j}$ and its time rate of change of $\dot{P}^1_{c_j}$ through the interface $\tilde{\Gamma}^j_1$ as

$$\dot{P}^1_{c_j} + \tau_0 P^1_{c_j} \doteq -\left\{ \begin{array}{l} \left\langle \frac{\partial^2 \zeta}{\partial t^2}, \phi_j \right\rangle_{\Delta^j_1} + \left\langle \tau_0 \frac{\partial \zeta}{\partial t}, \phi_j \right\rangle_{\Delta^j_1} + \left\langle gh \frac{\partial \zeta}{\partial x}, \frac{\partial \phi_j}{\partial x} \right\rangle_{\Delta^j_1} + \left\langle gh \frac{\partial \zeta}{\partial y}, \frac{\partial \phi_j}{\partial y} \right\rangle_{\Delta^j_1} \\ \quad - \left\langle J_x, \frac{\partial \phi_j}{\partial x} \right\rangle_{\Delta^j_1} - \left\langle J_y, \frac{\partial \phi_j}{\partial y} \right\rangle_{\Delta^j_1} - \left\langle Q_x \frac{\partial \tau_0}{\partial x}, \phi_j \right\rangle_{\Delta^j_1} - \left\langle Q_y \frac{\partial \tau_0}{\partial y}, \phi_j \right\rangle_{\Delta^j_1} \end{array} \right\}. \tag{22}$$

Here we assume that node j does not lie on the boundary Γ, otherwise we must adjust Eq. (22) so that we use the appropriate boundary conditions set forth in the model specifications. We recognize the right hand quantity is a function of time and thus treat Eq. (22) as an ODE that we numerically solve using Huen's method, which is second order accurate. For discussion purposes we present the analytical solution $P^1_{c_j}(t)$, such that

$$P^1_{c_j}(t) = \mathrm{e}^{-\tau_0 t} \int_0^t \mathrm{e}^{\tau_0 s} \Psi^1_j(s) \mathrm{d}s + c, \tag{23}$$

where

$$\Psi^1_j(t) = -\left\{ \begin{array}{l} \left\langle \frac{\partial^2 \zeta}{\partial t^2}, \phi_j \right\rangle_{\Delta^j_1} + \left\langle \tau_0 \frac{\partial \zeta}{\partial t}, \phi_j \right\rangle_{\Delta^j_1} + \left\langle gh \frac{\partial \zeta}{\partial x}, \frac{\partial \phi_j}{\partial x} \right\rangle_{\Delta^j_1} + \left\langle gh \frac{\partial \zeta}{\partial y}, \frac{\partial \phi_j}{\partial y} \right\rangle_{\Delta^j_1} \\ \quad - \left\langle J_x, \frac{\partial \phi_j}{\partial x} \right\rangle_{\Delta^j_1} - \left\langle J_y, \frac{\partial \phi_j}{\partial y} \right\rangle_{\Delta^j_1} - \left\langle Q_x \frac{\partial \tau_0}{\partial x}, \phi_j \right\rangle_{\Delta^j_1} - \left\langle Q_y \frac{\partial \tau_0}{\partial y}, \phi_j \right\rangle_{\Delta^j_1} \end{array} \right\} \tag{24}$$

and $c = P^1_{c_j}(0)$. For most applications, the water surface is initially at rest, so that $c = 0$. The quantity $P^1_{c_j}(t)$ represents only a partial mass flux for element Δ^j_1, namely the contributions to the total flux associated with node j. Thus to find the total mass flux for element Δ^j_1, we sum the partial fluxes associated with the vertices of that element, $P^1(t) = \sum_{j=1}^3 P^1_{c_j}(t)$. It is not clear if this partial flux is physically realistic, certainly one can not get the flux across a single edge of an element with this method.

Notice that the solution of (23) is over the time interval $[0, t]$ while we are interested in the solution in the time interval $[t_{k-1}, t_k]$. To obtain a time integration over the desired time interval we subtract subsequent solutions, namely,

$$P^1_B(t_k) = P^1(t_k) - P^1(t_{k-1}), \tag{25}$$

and define $P^1_B(t_k)$ as a local mass flux for element Δ^1_j at time t_k.

To complete the derivation of P^n_B and to ensure consistency, we first must use the integration rules employed by ADCIRC for the components of $\Psi_j(t)$, given in Table 1, whereby $\Psi_j(t)$ becomes

$$\begin{aligned} \Psi_j(t) = &-\frac{A_1}{12}\left(\sum_{i=1}^3 \varphi_{i,j} \frac{\partial^2 \zeta_i}{\partial t^2} + \bar{\tau}_{01} \sum_{i=1}^3 \varphi_{i,j} \frac{\partial \zeta_i}{\partial t} \right) - \frac{g\bar{h}_1}{4A_1}\left(b_j \sum_{i=1}^3 \zeta_i b_i + a_j \sum_{i=1}^3 \zeta_i a_i \right) \\ &+ \frac{1}{2}\left(\bar{J}_{x1} b_j + \bar{J}_{y1} a_j + \bar{Q}_{x1} \sum_{i=1}^3 \tau_{0i} \frac{b_i}{3} + \bar{Q}_{y1} \sum_{i=1}^3 \tau_{0i} \frac{a_i}{3} \right). \end{aligned} \tag{26}$$

Finally we note that in solving the GWCE, ADCIRC uses a weighted three step semi-implicit time discretization procedure at $s-1$, s, and $s+1$. All the time steps are uniform in size, i.e. $\Delta t = t_s - t_{s-1}$. The time dependent quantities in Eq. (26) are approximated in the following way

Table 1
Relevant integration rules used in ADCIRC

$\left\langle \frac{\partial^2\zeta}{\partial t^2}, \phi_j \right\rangle_{\Delta_1^j} = \frac{A_1}{12}\sum_{i=1}^{3}\varphi_{i,j}\frac{\partial^2\zeta_i}{\partial t^2}$	$\left\langle J_x, \frac{\partial\phi_j}{\partial x} \right\rangle_{\Delta_1^j} = \frac{\bar{J}_{x1}}{2}b_j$
$\left\langle \tau_0\frac{\partial\zeta}{\partial t}, \phi_j \right\rangle_{\Delta_1^j} = \frac{A_1\bar{\tau}_{01}}{12}\sum_{i=1}^{3}\varphi_{i,j}\frac{\partial\zeta_i}{\partial t}$	$\left\langle J_y, \frac{\partial\phi_j}{\partial y} \right\rangle_{\Delta_1^j} = \frac{\bar{J}_{y1}}{2}a_j$
$\left\langle gh\frac{\partial\zeta}{\partial x}, \frac{\partial\phi_j}{\partial x} \right\rangle_{\Delta_1^j} = \frac{g\bar{h}_1}{4A_1}b_j\sum_{i=1}^{3}\zeta_i b_i$	$\left\langle Q_x\frac{\partial\tau_0}{\partial x}, \phi_j \right\rangle_{\Delta_1^j} = \bar{Q}_{x1}\sum_{i=1}^{3}\tau_{0i}\frac{b_i}{6}$
$\left\langle gh\frac{\partial\zeta}{\partial y}, \frac{\partial\phi_j}{\partial y} \right\rangle_{\Delta_1^j} = \frac{g\bar{h}_1}{4A_1}a_j\sum_{i=1}^{3}\zeta_i a_i$	$\left\langle Q_y\frac{\partial\tau_0}{\partial y}, \phi_j \right\rangle_{\Delta_1^j} = \bar{Q}_{y1}\sum_{i=1}^{3}\tau_{0i}\frac{a_i}{6}$

$$\frac{\partial^2\zeta_i}{\partial t^2} = \frac{\zeta_i^{s+1} - 2\zeta_i^s + \zeta_i^{s-1}}{\Delta t^2}, \tag{27a}$$

$$\frac{\partial\zeta_i}{\partial t} = \frac{\zeta_i^{s+1} - \zeta_i^{s-1}}{2\Delta t}, \tag{27b}$$

$$\zeta_i = \alpha_1\zeta_i^{s+1} + \alpha_2\zeta_i^s + \alpha_3\zeta_i^{s-1}, \tag{27c}$$

$$\bar{J}_{x1}, \bar{J}_{y1} = \bar{J}_{x1}^s, \bar{J}_{y1}^s, \tag{27d}$$

$$\bar{Q}_{x1}, \bar{Q}_{y1} = \bar{Q}_{x1}^s, \bar{Q}_{y1}^s, \tag{27e}$$

where, α_1, α_2, α_3, are the time weighting factors which are set by the user.

In terms of realizing perfect local mass conservation with this consistent flux, it is worth looking at the analytical solution to the total flux for element Δ_1^j, prior to time discretization, i.e. Eq. (23). We assume for the time being that τ_0 is constant on the element; this assumption is not prohibitive and is presently the default case for historical simulations using ADCIRC. For each element, we sum the partial mass flux associated with each node to get

$$P^1(t) = \sum_{j=1}^{3} P_{c_j}^1(t) = \sum_{j=1}^{3} e^{-\tau_0 t}\int_0^t e^{\tau_0 s}\Psi_j^1(s)\,ds = e^{-\tau_0 t}\int_0^t e^{\tau_0 s}\left(\sum_{j=1}^{3}\Psi_j^1(s)\right)ds. \tag{28}$$

Next we use the definition of $\Psi_j^1(t)$ and Eq. (14a) and (14b) to get

$$P^1(t) = e^{-\tau_0 t}\int_0^t e^{\tau_0 s}\left(-\left\langle\frac{\partial^2\zeta}{\partial s^2}, 1\right\rangle_{\Delta_1^j} - \left\langle\tau_0\frac{\partial\zeta}{\partial s}, 1\right\rangle_{\Delta_1^j}\right)ds. \tag{29}$$

Now we apply Leibniz's rule to switch the order of integration and differentiation along with the assumption that on the current element, τ_0 is constant, to obtain

$$P^1(t) = e^{-\tau_0 t}\int_0^t e^{\tau_0 s}\left(-\frac{\partial}{\partial s}\left\langle\frac{\partial\zeta}{\partial s}, 1\right\rangle_{\Delta_1^j} - \tau_0\left\langle\frac{\partial\zeta}{\partial s}, 1\right\rangle_{\Delta_1^j}\right)ds. \tag{30}$$

We recognize that the integrand is a result of a product rule differentiation, so upon rearrangement we get

$$P^1(t) = e^{-\tau_0 t}\int_0^t -\frac{\partial}{\partial s}\left(e^{\tau_0 s}\left\langle\frac{\partial\zeta}{\partial s}, 1\right\rangle_{\Delta_1^j}\right)ds. \tag{31}$$

By the Fundamental Theorem of Calculus, Eq. (31) collapses to a statement of local mass conservation, namely

$$P^1(t) = -\left\langle \frac{\partial \zeta}{\partial t}, 1 \right\rangle_{\Delta_1^j}. \tag{32}$$

Of course, when we do discretize Eq. (23) in time whereby we can no longer exactly perform the operations done to get Eqs. (30)–(32), we should not expect perfect local mass conservation. This is mainly due to the presence of numerical errors in the approximation of the second derivative of elevation with respect to time.

In Section 3.1 we developed a flux that is physically realistic, yet is not consistent with the finite element formulation of our problem and hence does not guarantee local mass conservation. In Section 3.2 we developed a flux that is consistent with the finite element formulation, but may not be physically realistic and still does not result in local mass conservation due to the required time discretizations. This leads us to examine another option for determining a consistent local mass flux for the GWCE.

3.3. A post-processed flux

The final flux, a post-processed flux, will only be discussed in the context of the GWCE and follows the ideas set forth in the work of Hughes et al. [6]. In their work, Hughes et al. [6] show another method for defining local fluxes in such a way as to be consistent with the finite element state, see also Oshima et al. [17]. As a result they are able to show that the continuous Galerkin finite element method when applied to conservation laws like Eq. (1), is locally conservative. This is accomplished through a post-processing of the original finite element statement. Their approach dispels a common and long held notion that the CG method is only globally conservative.

Their basic idea is to solve the original finite element statement first, then define an auxiliary flux for the global boundary, whereby they solve a modified finite element problem for this auxiliary flux. Once this is complete they solve modified local finite element problems for element level fluxes. The modifications consists of adding new boundary terms for the areas of interest, elements in our case. Furthermore, the original basis space $\mathcal{S}^N$ is enlarged by including all the weight functions w_n in $\hat{\mathcal{S}}^M$, when solving for element level fluxes. Using this procedure, Hughes et al. [6] show that the resulting fluxes are locally and globally conservative. One consequence of solving the additional problem for the fluxes, they point out, citing Babuška and Miller [1], is that these new fluxes have many desirable qualities about them, including superconvergence properties. Their work falls into a broader category of methods called ''goal-oriented error estimation'' or ''quantities of interest'' see for example [19,18,15], where estimates are obtained for integral functionals, such as mass flux in our case and lift or drag in aeronautical applications to list just a few.

By applying the ideas detailed in Hughes et al. [6] to the GWCE in an effort to preserve conservation and consistency, we need to solve a system of equations for not only the mass flux but also the time rate of change of the mass flux, e.g. quantities similar to those on the left hand side of Eq. (22). Both of these quantities taken together are necessary to achieve local conservation and maintain consistency with the GWCE-based finite element formulation. But what we desire is only the local mass flux. So a similar situation presents itself to the one we had in Section 3.2 where an ODE was solved in order to extract the mass flux quantity. The need to discretize in time would again result in a lack of local mass conservation.

As a word of caution, Hughes et al. [6] point out, that their post-processing technique is basically an L_2 projection which can result in spurious oscillations near discontinuities. If spurious oscillations are reintroduced using such a post-processing technique, then we have defeated the purpose of using the GWCE in the first place.

It is possible to use the ideas of Hughes et al. [6] to setup the post-processing procedure to solve for just the mass flux, i.e. pretend we are solving Eq. (1). This approach results in a locally conservative mass flux,

but is not consistent with the original equation solution from the GWCE and very well may reintroduce spurious oscillations. Therefore, even considering the method of Hughes et al. [6], we are not able to satisfy both consistency and local mass conservation for a GWCE-based model.

While the methodology laid down by Hughes et al. [6] for finding locally conservative fluxes is valuable, the resulting flux is relatively expensive to compute and is an element averaged quantity which is not useful for transport purposes. Furthermore, the lack of local mass conservation caused by the need to solve an ODE for the flux and the possibility of reintroducing spurious oscillations through Eq. (1) are counterproductive. Thus, for these reasons we do not derive the flux as proposed by Hughes et al. [6] for the GWCE, nor give any numerical examples of it.

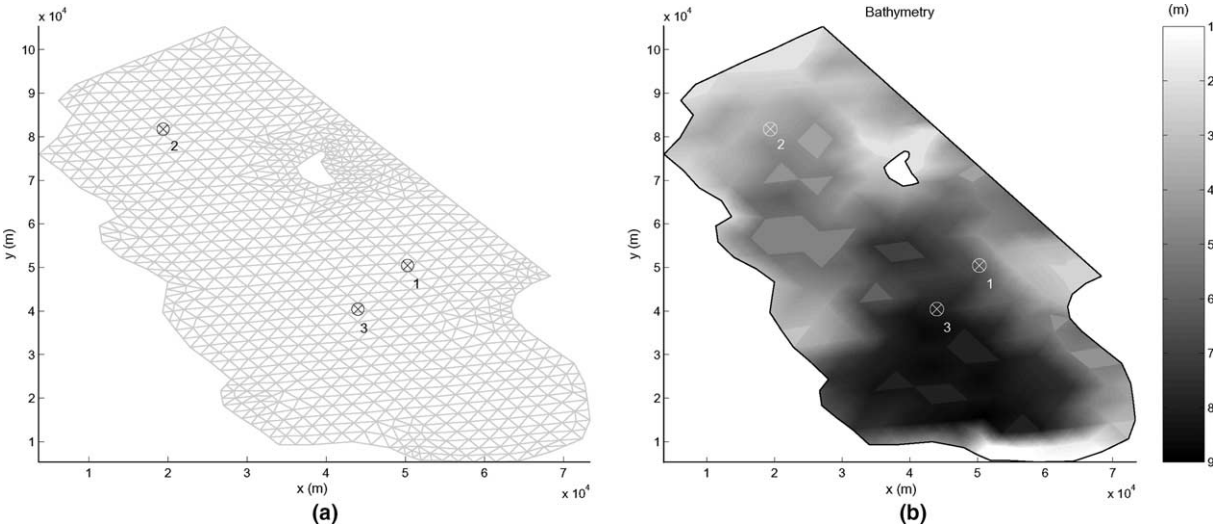

Fig. 3. The (a) mesh and (b) bathymetry in meters, for the Bight of Abaco, Bahamas with selected stations marked with a ⊗.

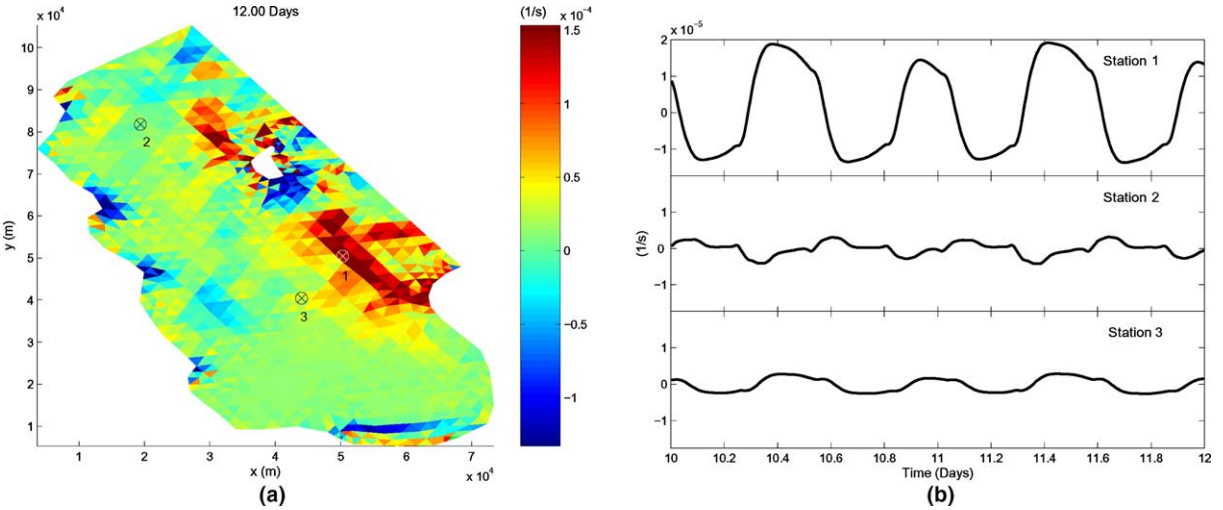

Fig. 4. For the Bight of Abaco, Bahamas: (a) Computed vorticity of the flow (1/s) at day 12.0 of the simulation with time-series stations marked with a ⊗ and (b) the time-series of vorticity at each station from day 10.0 to 12.0.

4. Numerical example

The finite volume flux, P_{fv}, and the consistent flux, P_B, defined in the previous sections for the GWCE-based finite element method employed by the coastal ocean circulation model ADCIRC, have been tested for a realistic coastal flow problem. The results of this test are presented below in an effort to support the analytical findings.

We present a realistic application for tidal circulation in the Bight of Abaco, Bahamas, which lies between the islands of Great Abaco to the east, Little Abaco to the north, and Grand Bahama to the west. This region is a site of significant nonlinear tidal generation due to its isolation from deep offshore waters (1000–2000 m) and its own very shallow depths. Tides propagate from open waters and are largely modified by frictional dissipation and nonlinear tidal interactions within the Bight.

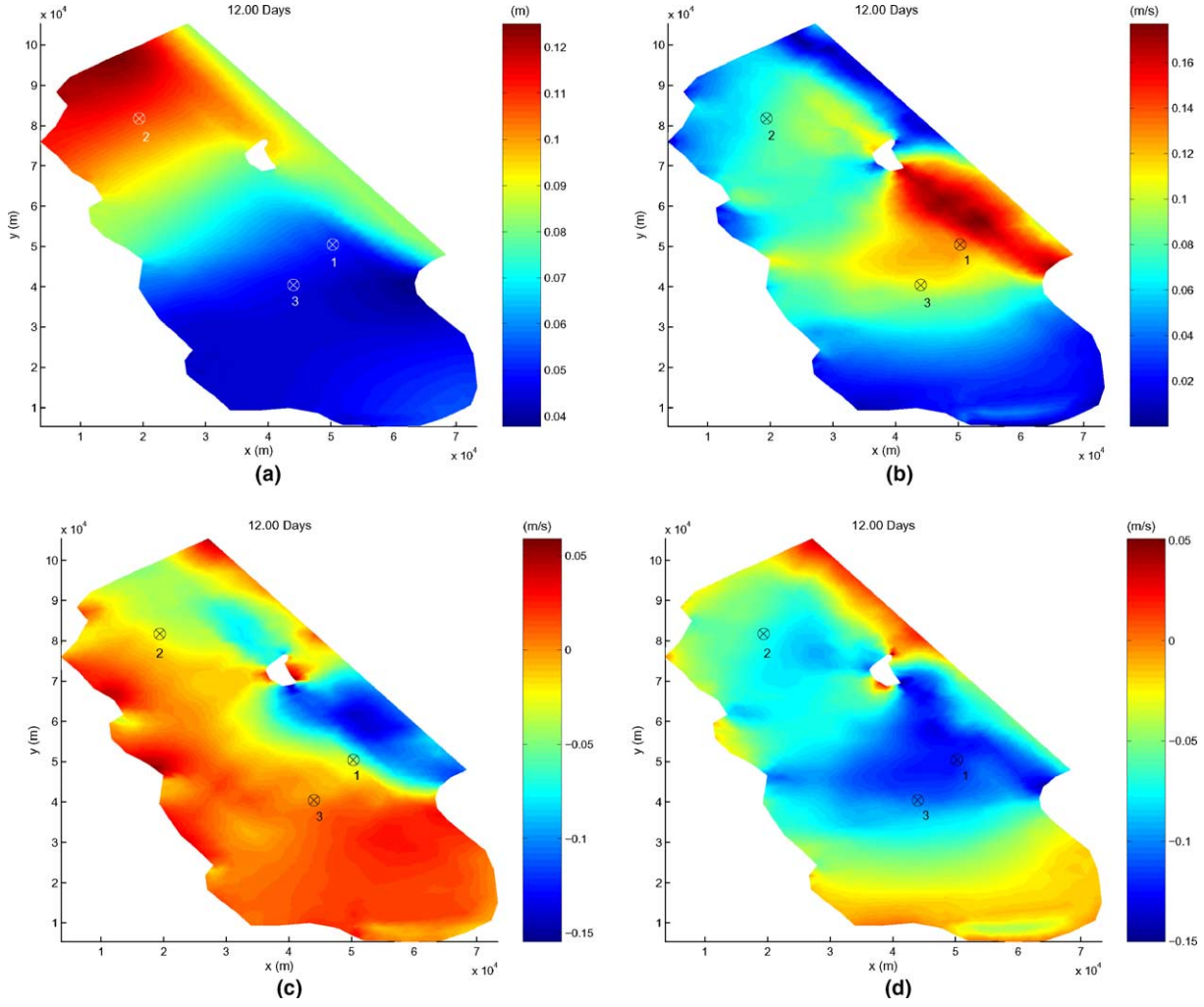

Fig. 5. For the Bight of Abaco, Bahamas: Computed (a) elevation (m), (b) magnitude of velocity (m/s), (c) magnitude of the x component of velocity (m/s), and (d) magnitude of the y component of velocity (m/s) at day 12.0 of the simulation with selected stations marked with a $\otimes$.

The basin is discretized by an unstructured triangular mesh using 1696 elements and 926 nodes, see Fig. 3a, such that the maximum element radius is 1750 m and the minimum element radius is 454 m (element radius being defined as the radius of the circle that circumscribes the element). The bathymetry varies from only 1.0 to 9.0 m as shown in Fig. 3b. Tidal forcings consisting of five primary constituents (K_1, O_1, M_2, S_2, and N_2) are applied at the open ocean boundary and are used to drive the 12-day simulation that includes a 5 day ramp period. A fixed time step value of 30 s. is used along with a GWCE parameter set to $\tau_0 = 0.01$. Lateral mixing effects are not considered.

For the Bight of Abaco simulation, the minimum and maximum elevation values over approximately four M_2 tidal cycles (day 10 to day 12) were −0.3622 and 0.4594 m, respectively. The x component of velocity ranges (from −0.4212 to 0.3594 m/s) and the y component of velocity ranges (from −0.3734 to 0.3140 m/s) with a resulting maximum magnitude of velocity of 0.4451 m/s. Fig. 5 presents a snapshot from day 12.0

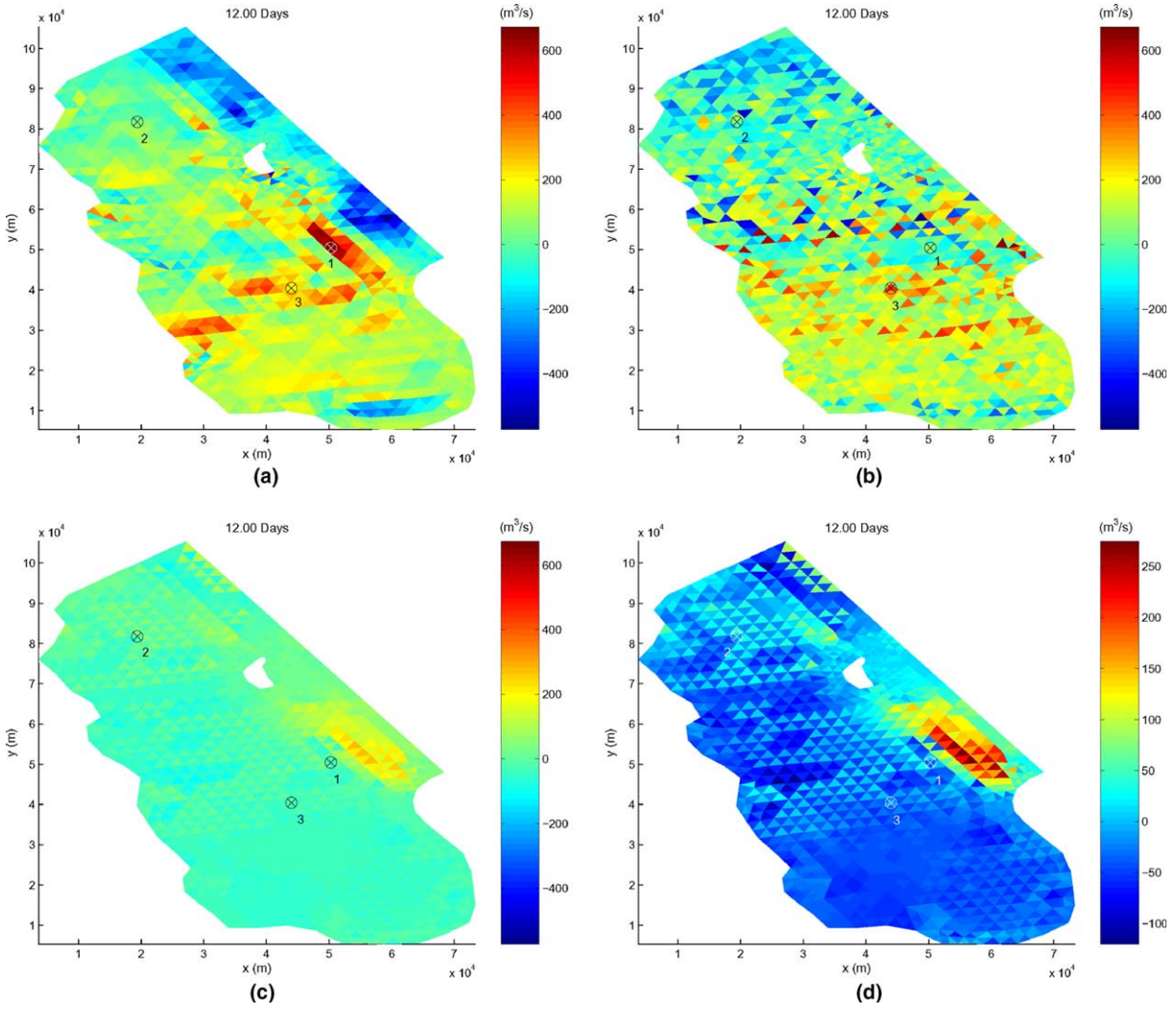

Fig. 6. For the Bight of Abaco, Bahamas: Computed fluxes (a) P_{fv}, the finite volume flux, and (b) P_B, the consistent flux, and their corresponding mass accumulation terms (c) and (d) $-\left\langle \frac{\partial \zeta}{\partial t}, 1 \right\rangle$ at day 12.0 of the simulation; selected stations are marked with a ⊗. Note that (c) and (d) are the same quantities viewed at different color scales.

Table 2
Invariant mesh and bathymetric information relevant to each of the station locations for the Bight of Abaco, Bahamas

Station #	Element area $(km)^2$	Node # i	Depth h_i (m)	$\|h_i - h_j\|_\infty$ (m)	Nodal radius (m)	Edge length (m)
1	2.7223	412	6.00	1.500	2687.4	2608.8
		440	4.75	1.500	2608.8	2522.1
		436	6.00	1.250	2687.4	2403.7
2	2.7083	792	3.75	0.500	2713.1	2534.5
		813	3.50	0.250	2713.1	2713.1
		809	3.25	0.500	2760.1	2304.9
3	2.7778	317	7.50	0.750	2833.3	2669.0
		336	7.25	0.500	2713.1	2687.4
		312	7.75	0.500	2833.3	2713.1

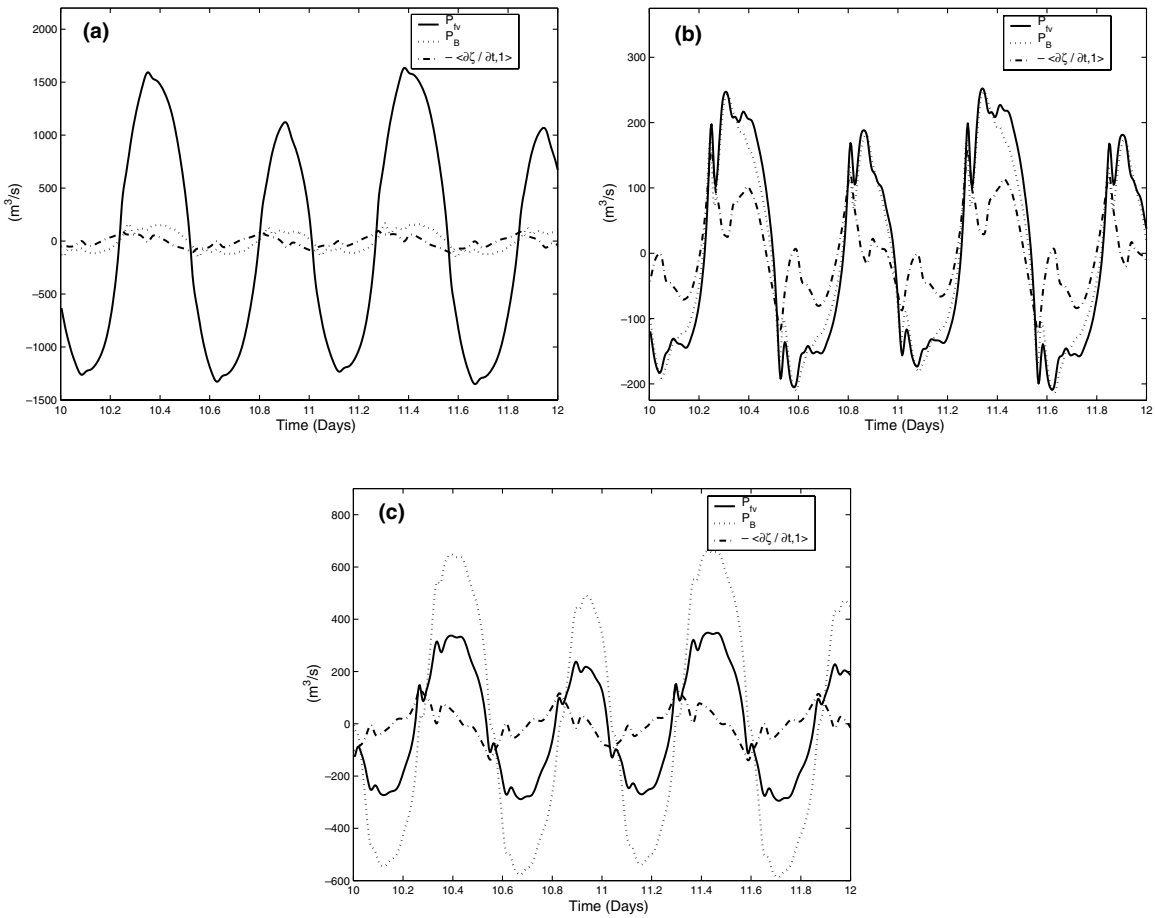

Fig. 7. For the Bight of Abaco, Bahamas: Comparisons of the finite volume flux P_{fv}, the consistent flux P_B, and the mass accumulation $-\left\langle \frac{\partial \zeta}{\partial t}, 1 \right\rangle$ in m^3/s for (a) station 1, (b) station 2, and (c) station 3.

of the computed elevation, magnitude of the velocity, and values of the x- and y-velocity components over the entire mesh, while Table 3 list the specific values of these quantities at the nodes of the three stations to be

discussed in more detail later. We also show the corresponding computed two-dimensional vorticity of the flow (1/s) in Fig. 4 for day 12.0.

For the same time period we present values of the local mass fluxes (m^3/s), computed as the finite volume flux, P_{fv} from Eq. (20) and the consistent flux P_B from Eq. (25) along with their corresponding mass accumulation terms $-\left\langle \frac{\partial \zeta}{\partial t}, 1 \right\rangle$ in Fig. 6. The color scales for Fig. 6a–c are fixed between -573 and 673 m^3/s in order to facilitate a direct comparison between the two flux measures. What is immediately obvious in the computed flux terms is that no apparent pattern emerges for the consistent flux values P_B, while the finite volume flux P_{fv} seems to track the tidal propagation in and out of the basin as shown in Fig. 5. However, neither flux balances their respective mass accumulation term $-\left\langle \frac{\partial \zeta}{\partial t}, w_n \right\rangle$, the consequence being that local mass is not conserved. Notice that the largest mass accumulation values in Fig. 6d occur roughly in the same regions where P_{fv} is largest in Fig. 6a. At these same locations the vorticity is also at its largest magnitude as seen in Fig. 4a. The correspondence between vorticity and local mass imbalance with respect to P_{fv} is discussed in more detail by Blain and Massey [2].

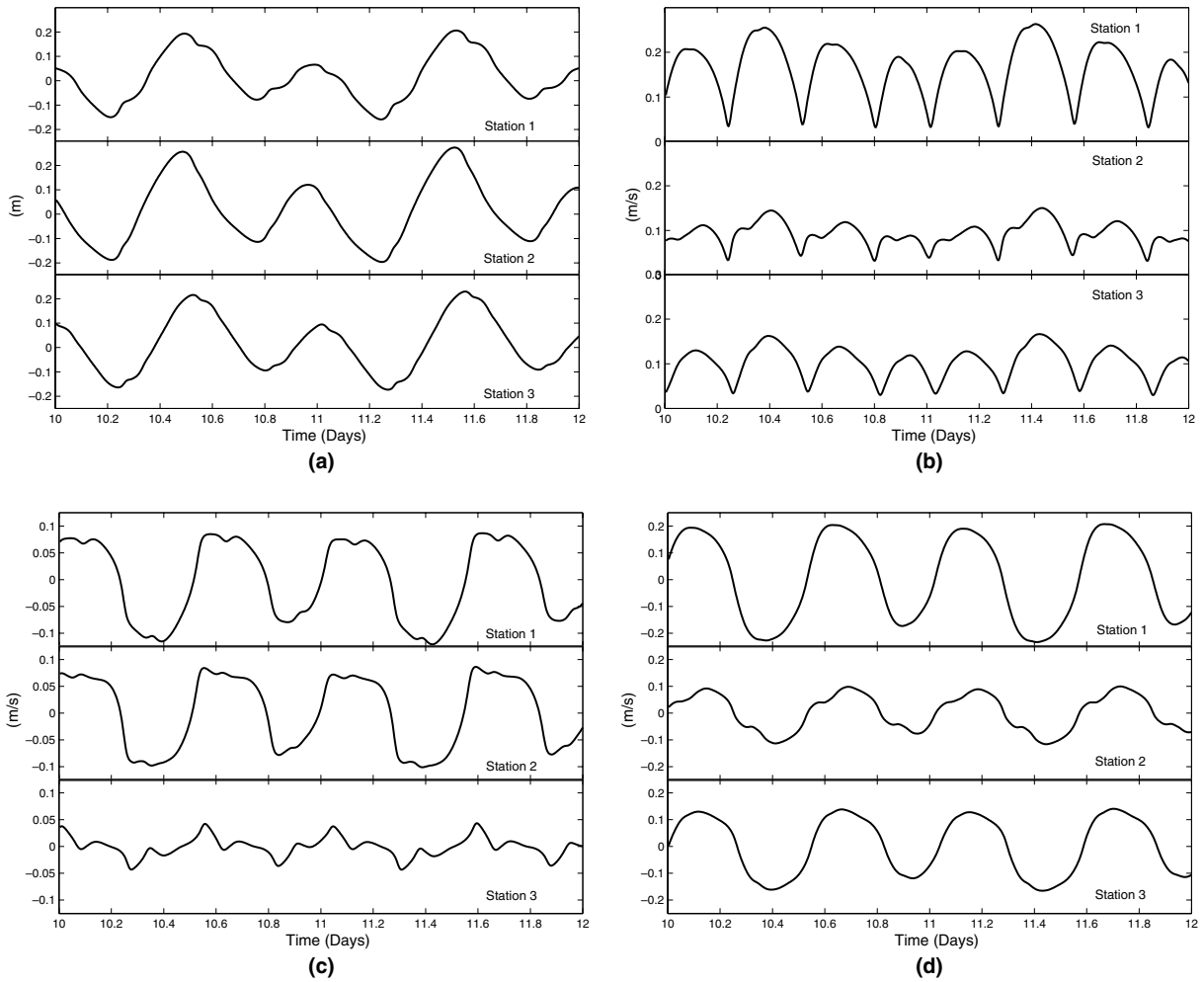

Fig. 8. For the Bight of Abaco, Bahamas: Comparisons of the element-averaged (a) elevation (m), (b) magnitude of velocity (m/s), (c) values of the x component of velocity (m/s) and (d) values of the y component of velocity (m/s) for each of the three stations.

Table 3
Information for the three stations at day 12.0 of the simulation for the Bight of Abaco, Bahamas

Station #	Node # i	ζ_i (m)	u_i (m/s)	v_i (m/s)
1	412	4.9848e-02	−2.7433e-02	−1.2202e-01
	440	5.0124e-02	−7.2452e-02	−1.2054e-01
	436	5.2335e-02	−3.1919e-02	−1.2376e-01
2	792	1.0706e-01	−2.4113e-02	−7.3052e-02
	813	1.0905e-01	−3.2615e-02	−7.2947e-02
	809	1.1022e-01	−2.4024e-02	−6.6203e-02
3	317	4.5431e-02	3.1354e-03	−1.0572e-01
	336	4.7007e-02	−3.1790e-03	−1.1093e-01
	312	4.6062e-02	2.3181e-03	−1.0037e-01

To examine the time behavior of these fluxes three stations are identified, see Fig. 3 for their locations, based on the local mass imbalances computed for each type of local mass flux considered. The relevant mesh and bathymetric details for each station are recorded in Table 2. Station 1 is an element having a high local mass imbalance when using the finite volume flux, P_{fv}. By contrast, station 2 has a low mass imbalance for either the finite volume, P_{fv}, or the consistent partial flux P_B. Lastly, station 3 is an element that has a high mass imbalance when using the consistent partial flux P_B. The time series behavior for each of the two fluxes at each station is shown in Fig. 7. Corresponding time series for the element averaged quantities of elevation (m), values of velocity (m/s) and the values of the x and y components of velocity (m/s) are shown in Fig. 8. Again, from Fig. 7, we see that neither of the computed fluxes balances the mass accumulation term $-\left\langle \frac{\partial \zeta}{\partial t}, w_n \right\rangle$ at any of the station locations. Both fluxes appear to have the same phase yet slightly different shapes at the extrema. Both fluxes are also out of phase with the mass accumulation term $-\left\langle \frac{\partial \zeta}{\partial t}, w_n \right\rangle$, especially at stations 1 and 3 where the flux values clearly lead the mass accumulation. The larger values of the finite volume flux, P_{fv} at station 1, are physically realistic based on a comparison of the velocity magnitudes at each of the three stations. Station 1 has a velocity magnitude that is nearly one and half times the magnitude of the velocity at the other two stations. Station 1 is also located within a region that experiences a relatively steep gradient in bathymetry as depths drop dramatically beyond the shallow sill at the entrance to the Bight of Abaco (see the nodal depths for station 1 in Table 2). Such steep bathymetric gradients are known to result in larger mass imbalances, see Oliveira et al. [16].

This numerical example illustrates that the finite volume flux, P_{fv}, is physically realistic even though it is not consistent with the finite element formulation. The finite volume flux is also a good indicator of where local mass imbalances are likely to occur. Additionally, we have shown that the consistent flux, P_B, is not physically based and does not always predict regions where local mass imbalances would occur. We feel that for the GWCE, the finite volume flux, P_{fv}, should be retained as an analysis tool.

5. Conclusions

We examined three ways of computing local mass flux and the resulting mass balance for the coastal ocean circulation model, ADCIRC, which uses the GWCE in order to control $2\Delta x$ spurious waves. We have shown that none of the fluxes discussed satisfy all three desired traits of being, physically realistic, locally mass conservative, and consistent with the finite element statement being solved. We have shown that the most straight forward way of computing fluxes, the finite volume flux, P_{fv}, gives physically realistic results. We hope that this paper has added clarity to the concept of local conservation with respect to continuous Galerkin finite element statements.

Acknowledgement

The funding for this research has come from the Office of Naval Research, Naval Ocean Modeling Program, Award No. N00014-02-WX-20834, "Improvements to the Conservation Properties of FE-Based Models." Part of this work was performed while the first author held a National Research Council Research Associateship Award with the Naval Research Laboratory at Stennis Space Center. This work is Naval Research Laboratory contribution number NRL/JA/7320/04/0011.

References

[1] I. Babuška, A. Miller, The post-processing approach in the finite element method. 1. Calculation of displacements, stresses and other higher derivatives of the displacements, Int. J. Numer. Methods Engrg. 20 (1984) 1085–1109.
[2] C.A. Blain, T.C. Massey, Application of a coupled discontinuous–continuous Galerkin finite element shallow water model to coastal ocean dynamics, Ocean Modelling, in press.
[3] R.C. Berger, S.E. Howington, Discrete fluxes and mass balance in finite elements, J. Hydraulic Engrg. 128 (2002) 87–92.
[4] D.B. Haidvogel, A. Beckmann, Numerical Ocean Circulation Modeling, Imperial College Press, London, 1999.
[5] J.L. Hench, R.A. Luettich, Analysis and application of Eulerian finite element methods for the transport equation, in: M.L. Spaulding, A.F. Blumberg (Eds.), Estuarine Coastal Modeling, Proceedings of Fifth International Conference, ASCE, Reston, Virginia, 1998.
[6] T.J.R. Hughes, G. Engel, L. Mazzei, M.G. Larson, The continuous Galerkin method is locally conservative, J. Computat. Phys. 163 (2000) 467–488.
[7] I. Kinnmark, The Shallow Water Wave Equations: Formulation, Analysis, and ApplicationLecture Notes in Engineering, vol. 15, Springer-Verlag, Berlin, 1986.
[8] R.L. Kolar, J.J. Westerink, M.E. Cantekin, C.A. Blain, 1994: Aspects of nonlinear simulations using shallow-water models based on the wave continuity equation, Comput. Fluids 23 (1994) 523–538.
[9] R.L. Kolar, J.J. Westerink, A look back at 20 years of GWCE-based shallow water models, in: L.R. Bentley et al. (Eds.), Computational Methods in Water Resources, XIII, 2, Surface Water Systems and Hydrology, A.A. Balkema, Rotterdam, 2000.
[10] D.Y. Le Roux, A. Staniforth, C.A. Lin, Finite elements for shallow-water equation ocean models, Monthly Weather Rev. 126 (1998) 1931–1951.
[11] R.A. Luettich, J.J. Westerink, N.W. Scheffner, ADCIRC: An advanced three-dimensional circulation model for shelves, coasts, and estuaries, Report 1: Theory and methodology of ADCIRC-2DDI and ADCIRC-3DL, Technical Report DRP-92-6, USAE, Vicksburg, MS, 1992, 137 p.
[12] R.A. Luettich, J.C. Muccino, M.G.G. Foreman, 2002: Considerations in the calculation of vertical velocity in three-dimensional circulation models, J. Atmospheric Oceanic Technol. 19 (2002) 2063–2076.
[13] R.A. Luettich, J.J. Westerink, Formulation and numerical implementation of the 2D/3D ADCIRC finite element model Version 43.XX, 2003 [Available online at http://www.marine.unc.edu/C_CATS/adcirc/adcirc.htm].
[14] D.R. Lynch, J.T.C. Ip, C.E. Naimie, F.E. Werner, 1996: Comprehensive coastal circulation model with application to the Gulf of Maine, Continental Shelf Res. 16 (1996) 875–906.
[15] J.T. Oden, S. Prudhomme, Goal-oriented error estimation and adaptivity for the finite element method, Comput. Math. Appl. 41 (2001) 735–756.
[16] A. Oliveira, A.B. Fortunato, A.M. Baptista, Mass balance in Eulerian–Lagragian transport simulations in estuaries, J. Hydraul. Engrg. 126 (2000) 605–614.
[17] M. Oshima, T.J.R. Hughes, K. Jansen, Consistent finite element calculations of boundary and internal fluxes, Int. J. Comput. Fluid Dyn. 9 (1998) 227–235.
[18] N.A. Pierce, M.B. Giles, Adjoint recovery of superconvergent functionals from PDE approximations, SIAM Rev. 42 (2000) 247–264.
[19] S. Prudhomme, J.T. Oden, On goal-oriented error estimation for elliptic problems: application to the control of pointwise errors, Comput. Methods Appl. Mech. Engrg. 176 (1999) 313–331.